Diffuse Correlation Spectroscopy (DCS): A Diagnostic Tool for Assessing Tissue Blood Flow in Vascular-Related Diseases and Therapies

Guoqiang Yu*

Center for Biomedical Engineering, University of Kentucky, 600 Rose Street, Lexington, KY 40506-0070, USA

Abstract: The development and clinical application of a novel near-infrared diffuse correlation spectroscopy (DCS) have been reviewed in this paper. DCS measures speckle fluctuations of near-infrared diffuse light in tissue, which are sensitive to the motions of red blood cells. DCS offers several new features which make it appealing for blood flow measurement such as noninvasiveness, high temporal resolution (up to 100 Hz), portability, and relatively large penetration depth (up to ~1.5 centimeters). DCS technology can be utilized for bedside monitoring of tissue blood flow as exemplified by applications involving tumors, brains, and skeletal muscles. In these investigations, DCS measurements show promise for quantification of tissue hemodynamic status, for diagnosis of vascular-related diseases (e.g., cancers, stroke, peripheral arterial disease), and for continuous monitoring and evaluation of therapeutic effects (e.g., chemotherapy, radiation therapy, photodynamic therapy, arterial revascularization).

Keywords: Near-infrared Spectroscopy (NIRS), Diffuse Correlation Spectroscopy (DCS), Microvascular Blood Flow, Diagnosis of Vascular Disease, Noninvasive Therapeutic Monitoring.

1. INTRODUCTION

1.1. Various Diseases Associated with Abnormal Blood Flow

Blood flow is one of the most important physiological factors affecting delivery of O_2 and other nutrients to tissues. Many diseases are associated with abnormal blood flow such as stroke, peripheral arterial disease (PAD), and cancer [1-5]. An occlusive stroke/PAD is an interruption of the blood supply (flow) to the brain/skeletal muscle, which may impair or even destroy the cerebral/muscular function. The abnormal vasculature in tumors may generate abnormal tumor blood flow compared to the surrounding normal tissues. The various treatments for these diseases share the common goal of modifying blood flow in some way. These treatments include improving blood flow to the ischemic tissues or shutting down the blood flow to cancer cells. Therefore, measurement of tissue blood flow may provide information for diagnosis of various tissue diseases, and for monitoring of therapeutic effects.

Blood flow, however, is difficult to measure accurately because measurement sensitivity and stability depends on the magnitude of flow, location and the diameter of the individual vessels that vary over a wide range; e.g., vessel diameters range from 2 cm (major arteries or veins) down to several micrometers (capillaries). In the clinic, measurements are required to be noninvasive, continuous, and fast while still providing accurate and useful quantitative flow information in macro- and micro-vasculature of deep tissues.

*Address correspondence to this author at the Center for Biomedical Engineering, University of Kentucky, 600 Rose Street, Lexington, KY 40506-0070, USA; Tel: 859-257-9110; Fax: 859-257-1856;
E-mail: Guoqiang.yu@uky.edu

1.2. Various Noninvasive Techniques for Measurement of Blood Flow

A variety of noninvasive methods are currently used for the measurement of blood flow and velocity [6]. Doppler ultrasound, for example, employs the Doppler effect to assess whether blood is moving towards or away from the probe, and its relative velocity. Duplex ultrasonography can image large and deep vessels in three dimensions with relatively high spatial (~mm) and temporal (~ms) resolution. However, this technique is limited to large vessels.

Other Imaging modalities for evaluation of blood flow in deep tissues at the level of the microvasculature [6] include positron emission tomography (PET) [7], single photon emission computed tomography (SPECT) [8], Xenon-enhanced computed tomography (XeCT) [9], dynamic perfusion computed tomography (PCT) [10], dynamic susceptibility contrast magnetic resonance imaging (DSC-MRI) [11], and arterial spin labeling MRI (ASL-MRI) [12, 13]. These techniques use endogenous (ASL-MRI) or exogenous tracers (PET, SPECT, XeCT, PCT, DSC-MRI), and their temporal and spatial resolutions vary. For example, the data acquisition time for ASL-MRI, PCT and DSC-MRI is in the range of seconds to minutes, approximately 10 times faster than the other techniques mentioned above. The spatial resolution for PCT, DSC-MRI and ASL-MRI can be as small as 2 mm and is typically better than that of the other techniques, i.e., 4-6 mm. However, these imaging modalities have several limitations that preclude their routine use in clinics. PET, SPECT, and Xenon-CT require exposure to ionizing radiation, and PET and SPECT require arterial blood sampling for quantification of blood flow. The MRI methods cannot be used in patients with pacemakers, metal implants, or claustrophobia. Furthermore, most of these methods require large and costly

1875-6603/12 $58.00+.00 ©2012 Bentham Science Publishers

instrumentation, and are largely incompatible with serial/continuous measurements.

Other surface-sensitive imaging techniques for measurement of microvascular flow include scanning laser Doppler [14], laser speckle imaging [15, 16], and Doppler optical coherence tomography (DOCT) [17]. These methods are used primarily for noninvasive monitoring of blood flow in tissues located at a few hundred microns below the tissue surface.

From the discussion above, there is apparently a critical need to develop bedside techniques that can monitor microvascular blood flow in deep tissues noninvasively, frequently, and relatively inexpensively.

1.3. "Static" Near-infrared Spectroscopy (NIRS) for Measurement of Deep Tissue Hemodynamics

A well known spectral window exists in the near-infrared (NIR, 700-900 nm) wherein tissue absorption is relatively low so that light can penetrate into deep/thick volumes of tissue (up to several centimeters). Near-infrared spectroscopy (NIRS) provides a fast and portable alternative to costly imaging techniques (e.g., MRI, CT) for measurement of deep tissue hemodynamics at the level of microvasculature. However, NIRS has relatively poor spatial resolution when probing deep tissues: ~0.5 mm near the surface and the resolution degrades with depth.

Traditional NIRS is a "static" method; it primarily measures the relatively slow variations in tissue absorption and scattering, as well as the derived values of hemoglobin concentration and blood oxygen saturation [18-39]. Very fast NIRS methods [40, 41] have been employed to measure rapid (~100 Hz) changes in tissue scattering. Nevertheless, these methods are still referred to as "static" since they investigate changes in the "amount of scattering" rather than the motion of the scatterer.

The most common applications of NIRS focus on the continuous measurements of hemoglobin concentration and blood oxygen saturation. NIRS has also been used to indirectly estimate blood flow using an exogenous tracer (e.g., Indocyanine Green) in deep/thick volume of tissues [42, 43]. This method, however, is minimally invasive as it requires intravenous injection of Indocyanine Green (ICG).

1.4. "Dynamic" NIR Diffuse Correlation Spectroscopy (DCS) for Measurement of Deep Tissue Blood Flow

Recently, a new "dynamic" NIR technique (namely diffuse correlation spectroscopy (DCS) or diffuse wave spectroscopy (DWS)) was developed which can directly measure the motions of scatterers while also maintaining all the advantages of NIRS [44-52]. In the case of tissues, the primary moving scatterers are red blood cells (RBCs). DCS offers several attractive new features for blood flow measurement such as noninvasiveness (i.e., no ionizing radiation, no contrast agents, no occlusion disturbance), high temporal resolution (up to 100 Hz) [53], portability, and relatively large penetration depth (up to ~1.5 centimeters) [54, 55]. Furthermore, DCS can be easily and continuously applied at the bed-side in the clinic [2, 3].

DCS measurements of blood flow variation in various tissues/organs have been successfully validated against other standards, including power Doppler ultrasound in murine tumors [5, 56], laser Doppler in rat brain [57], Xenon-CT in traumatic brain [58], Doppler ultrasound in premature infant brain [59, 60], fluorescent microsphere measurement of cerebral blood flow in piglet brain [1], and ASL-MRI in human brain and muscle [55, 61], and have been compared to reports in the literature [53, 57, 62-66]. This validation research has progressed hand-in-hand with numerical, theoretical studies [50, 57, 67-71], and with studies of tissue simulating phantoms [57, 68, 72, 73]. Overall, these studies have shown that DCS measurements of blood flow variations are in good agreement with theoretical expectation, computer simulation, and other biomedical measurement techniques.

The utility of DCS technology for bedside monitoring of tissue blood flow has been recently demonstrated in tumors [3, 5, 56, 65, 74-77], brains [57, 63, 66, 71, 78], and skeletal muscles [4, 61, 79-82]. The early stages of many of these studies focused on blood flow in animal models (e.g., murine tumors [5, 56], rat and piglet brains [1, 63, 64, 71], pig limb muscles [83]). More recently, the DCS technique has been a key component in a variety of clinical studies (e.g., human cancers of prostate [3], breast and head & neck [65, 75, 76, 84], cerebral functional activities [55, 78], cerebral stroke [2], traumatic brain injury [58], skeletal muscle physiology [4, 80-82]). In these preclinical and clinical investigations, DCS was used for quantification of tissue hemodynamic status, for diagnosis of disease, and for continuous monitoring and evaluation of therapeutic effects. In some of these studies, DCS was combined with NIRS in hybrid instruments and simple models were used to estimate tissue oxygen metabolism ($TMRO_2$) from the measured flow and oxygenation data [84]. This metabolic index is potentially a more direct indicator of tissue metabolic activities which integrates many factors and provides further insight about tissue physiology.

This review paper first outlines the historical development, basic principles and general instrumentation of DCS. It then focuses on introducing some *clinical* application examples of DCS.

2. DCS TECHNOLOGY

2.1. Historical Development of DCS Technology

The dynamic (or correlation) methods detect the motion of scatterers, typically starting with a system employing coherent sources and single photon counting detectors. The temporal statistics (or frequency-domain analogs of temporal statistics) of the fluctuations of the scattered light within a single speckle area are then monitored. In most of these dynamic experiments, the electric field temporal autocorrelation function or its Fourier transform is measured. Using a model for photon propagation through tissues, this measured signal can then be related to the motion of the RBCs and, consequently, blood flow can be determined.

Early physiological work from tissues utilized single-scattering theory [46, 47, 51], [85-87] to analyze data using pairs of very closely separated (< 1 mm) optodes, e.g., Laser Doppler flowmetry and charge-coupled device (CCD)-based

speckle devices [46, 51, 88]. Most of these measured light fluctuations in superficial tissue (< 1 mm). The single-scattering approximation simplifies the experimental analysis, but also limits the reliability and amount of information that can be extracted from real deep tissue samples.

Extension to highly scattering systems was made in the 1980's in various guises [45, 48, 49, 52]. The analogy of correlation transport to photon transport was made in the 1990's in order to better understand the behavior of correlation functions in the regime between single scattering and multiple scattering. Particularly, a diffuse correlation theory (DCS) for predicting speckle fluctuations of the highly scattered light was first introduced by Yodh and Boas in 1995 [44, 50, 89]. A diffusion equation unifying earlier models that describes the transport of the electric field temporal autocorrelation function through turbid media was derived, providing a mathematical description about how motional fluctuations are impressed upon the temporal correlations of diffuse light fields propagating in tissue. The advantage of the correlation diffusion theory over previous theories is the ease with which predictions can be made for turbid media with spatially varying dynamics and optical properties. As a result of these accomplishments, the DCS theory and instrumentation have been developed to optically probe blood flow in thick tissues [2-5, 55, 64, 65, 71, 75, 84, 90].

2.2. DCS Principles

DCS is an extension of single-scattering dynamic light scattering (DLS) (or quasi-elastic light scattering, QELS) to the multiple scattering limit. In a single scattering *thin* sample, photons are usually scattered once (or not at all) before they leave the sample. If the scatterers are particle-like objects that move, then the total electric field will vary in time and intensity fluctuations are observed. The fluctuations of the electric field and intensity carry information about the dynamic properties of the medium, i.e., the motion of the particles. In most experiments, the electric field temporal autocorrelation function or its Fourier transform is measured.

In applications involving most biological *thick* tissues, single-scattering theory becomes inadequate as multiple scattering effects must be accounted for. In this case, each scattering event from a moving scatterer contributes to the accumulation of the phase shift and therefore the decay of the correlation function. The fields from individual photon paths are assumed to be uncorrelated so that, subsequently, the total temporal field autocorrelation function can be expressed as the weighted sum of the field autocorrelation function from each photon path.

Boas *et al* derived a correlation diffusion equation describing the propagation of the unnormalized electric field temporal autocorrelation function in turbid (multiple scattering) media [44, 50, 91], based on correlation transport theory [92, 93]. This differential equation approach is particularly attractive for investigation of heterogeneous media [44, 50, 94] and provides a natural framework for tomographic reconstruction of tissue flow dynamics [44, 63, 71]. Details of the correlation diffusion equation derivation can be found elsewhere [44, 50, 91]. This review paper does not reproduce the earlier derivations, but instead simply introduces the well-known diffusion equation for photon fluence rate, and then writes out the analogous result for photon electric field correlation. Interested readers are strongly encouraged to consult primary references and recent reviews for more details.

In highly scattering media such as tissue, the photon fluence rate, $\Phi(\mathbf{r},t)$ [Watt· cm^{-2}], obeys the time-dependent diffusion equation:

$$\nabla\cdot(D\nabla\Phi(\mathbf{r},t))-v\mu_a\Phi(\mathbf{r},t)+vS(\mathbf{r},t)=\frac{\partial\Phi(\mathbf{r},t)}{\partial t} \qquad (1)$$

where $\boldsymbol{r}$ is the position vector, t [s] is time, and v [cm· s^{-1}] is the speed of light in the medium. μ_a [cm^{-1}] is the medium absorption coefficient, and $D\approx v/3\mu_s'$ is the photon diffusion coefficient in the medium, where μ_s' [cm^{-1}] is the reduced scattering coefficient of the medium. $S(\mathbf{r},t)$ [Watt· cm^{-3}] is the isotropic source term.

Using essentially the same set of approximations, the *unnormalized* temporal field autocorrelation function, $G_1(\mathbf{r},\tau)=\langle\mathbf{E}(\mathbf{r},t)\cdot\mathbf{E}^*(\mathbf{r},t+\tau)\rangle$, obeys a formally similar diffusion equation, i.e.,

$$\nabla\cdot(D\nabla G_1(\mathbf{r},\tau))-(v\mu_a+\tfrac{1}{3}v\mu_s'k_0^2\langle\Delta r^2(\tau)\rangle)G_1(\mathbf{r},\tau)=-vS_0e^{i\omega\tau}\delta^3(\mathbf{r}-\mathbf{r}_s) \qquad (2)$$

Here the source term is continuous wave (CW), τ is the autocorrelation delay time, ω is the angular frequency of the input light field, $k_0=\frac{2\pi n}{\lambda}$ is the wavevector magnitude of the incident light field, n is the index of refraction of the medium, λ is the wavelength of the light field, and $\langle\Delta r^2(\tau)\rangle$ is the mean square displacement of the scatterers in the medium, which directly characterizes the scatterer movement.

The scatterer movement (i.e., $\langle\Delta r^2(\tau)\rangle$) combines with photon absorption to give an *effective* "absorption" term for the attenuation of unnormalized electric field temporal autocorrelation function as it travels through the medium. The recognizable similarity of Equation 1 and Equation 2 suggests that they will have similar solutions. In semi-infinite homogeneous media (see Fig. (**1**)), for example, the solution to Equation 2 can be obtained as [91],

$$G_1(\rho,\tau)=\frac{vS_0e^{i\omega\tau}}{4\pi D}\left(\frac{e^{-K(\tau)r_1}}{r_1}-\frac{e^{-K(\tau)r_2}}{r_2}\right) \qquad (3)$$

Here, ρ is the distance between the source and detector fibers, $r_1=\sqrt{\rho^2+z_0^2}$, $r_2=\sqrt{\rho^2+(z_0+2z_b)^2}$, $z_0=\frac{1}{\mu_s'}$, $z_b=\frac{2}{3\mu_s'}\frac{1+R_{eff}}{1-R_{eff}}$, $R_{eff}=-1.44n^{-2}+0.71n^{-1}+0.668+0.064n$ is the effective

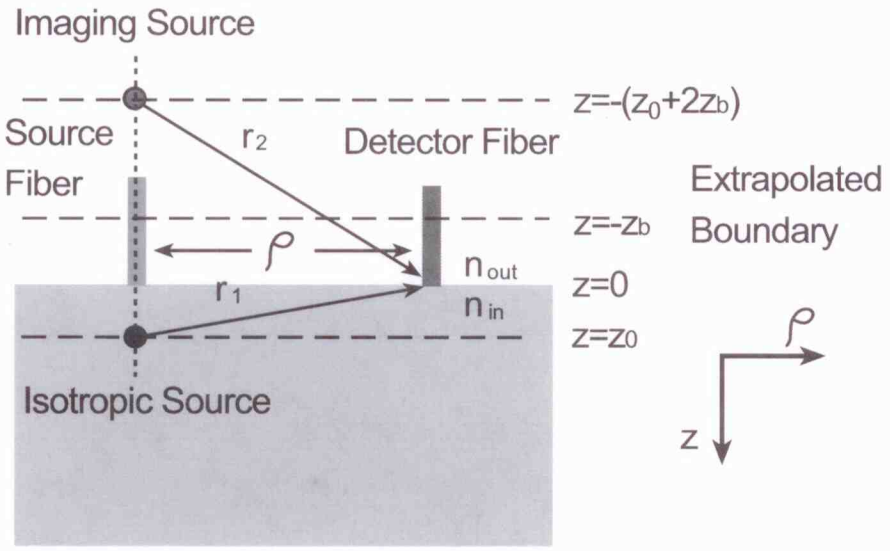

Fig. (1). Illustration of the semi-infinite geometry. The collimated source is usually approximated as an isotropic source located at $z = z_0 = 1/\mu_s'$ into the medium. The boundary condition requirement leads to a signal size of zero for the temporal autocorrelation function at $z = -z_b = -\frac{2}{3\mu_s'}\frac{1+R_{eff}}{1-R_{eff}}$, which is generally called the extrapolated zero boundary condition [115]. For the semi-infinite homogeneous geometry, the extrapolated zero boundary condition can be satisfied by considering a negative isotropic imaging source located at $z = -(z_0 + 2z_b)$. Courtesy of C. Zhou [68].

reflection coefficient defined by the ratio of the refraction indices inside and outside the medium ($n = n_{in} / n_{out}$, see Fig. (**1**)), and $K^2(\tau) = 3\mu_a\mu_s' + \mu_s'^2 k_0^2 \langle \Delta r^2(\tau) \rangle$.

For biological tissues there is another required modification of the correlation diffusion equation. Generally, biological tissues contain *static* (or very slow moving) scatterers (e.g., organelles, mitochondria, etc.) and *moving* scatterers (e.g., RBCs). The scattering events from the static objects in tissue do not contribute significantly to the phase shift and correlation function temporal decay in Equations 2. To account for this effect, a unitless factor, α (ranging from 0 to 1), is introduced to represent the fraction of light scattering events from "moving" scatterers. The factor α is included as a pre-fix to the *effective* ''absorption'' term in Equation 2 (i.e., $\frac{1}{3}v\mu_s' k_0^2 \alpha \langle \Delta r^2(\tau) \rangle$), and so it arises as well as in the definition of $K^2(\tau)$ (i.e., $K^2(\tau) = 3\mu_a\mu_s' + \mu_s'^2 k_0^2 \alpha \langle \Delta r^2(\tau) \rangle$). The decay of the temporal field correlation function thus depends on tissue optical properties, μ_a, μ_s', $\langle \Delta r^2(\tau) \rangle$, and the factor α which accounts for the presence of static scatterers.

For the case of random ballistic flow, $\langle \Delta r^2(\tau) \rangle = V^2\tau^2$, where V^2 is the second moment of the cell velocity distribution. For the case of diffusive motion, $\langle \Delta r^2(\tau) \rangle = 6D_b\tau$, where D_b is the *effective* Brownian diffusion coefficient of the tissue scatterers, and is distinct from the well known thermal Brownian diffusion coefficient defined originally by Einstein [95]. Red blood cells (RBCs) pass through capillaries in single file and experience shear flow in larger vessels; the RBCs also experience tumbling motions in addition to translation. Intuitively, the random ballistic flow model might be considered the best model with which to fit DCS data. In practice, however, the diffusion model, i.e., $\langle \Delta r^2(\tau) \rangle = 6D_b\tau$, fits the auto-correlation curves rather well over a broad range of tissue types (see Fig. (**2**)), ranging from rat brain [64, 71] and mouse tumor [5, 56], to piglet brain [1], adult human skeletal muscle [4, 79], adult human tumors [75, 84], premature brain [59, 60], and adult brain [2, 54, 55, 62]. There is currently no evidence explaining why Brownian-motion like correlation curves work effectively and more investigations are needed to resolve these issues. Nevertheless, an empirical approach has been adopted by researchers in biomedical optics applying DCS for measurement of tissue blood flow.

Although the unit of αD_b (cm^2/s) differs from the traditional blood perfusion unit [ml/min/100 g], changes in αD_b have been found to correlate quite well with other blood flow measurement modalities as described above. Therefore, αD_b is used as the blood flow index ($BFI = \alpha D_b$). $rBF = \frac{BFI}{BFI_0}$ is used to indicate relative blood flow changes, where BFI_0 is the DCS flow measurement at the baseline.

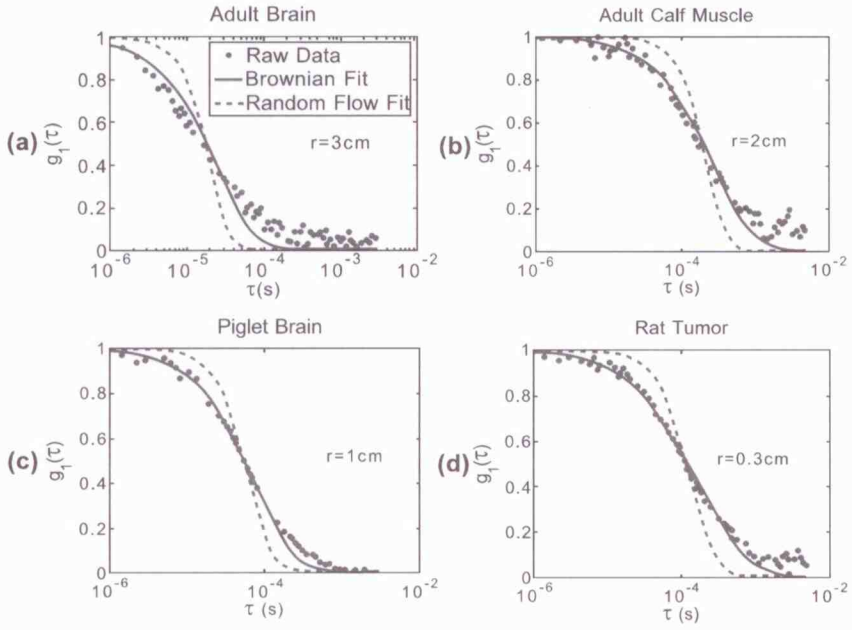

Fig. (2). DCS data (i.e., the normalized electric field autocorrelation function) from an adult human brain (**a**), human calf muscle (**b**), piglet brain (**c**), and rat tumor (**d**). The source-detector separations are also indicated on each plot. Dots are experimental data. The dashed line is a fit with $<\Delta r^2> \sim \tau^2$ (random flow), and the solid line is a fit with $<\Delta r^2> \sim \tau$ (Brownian motion). The diffusion model (Brownian motion) fits the auto-correlation curves better than the random flow model over a broad range of tissue types. Courtesy of C. Zhou [68].

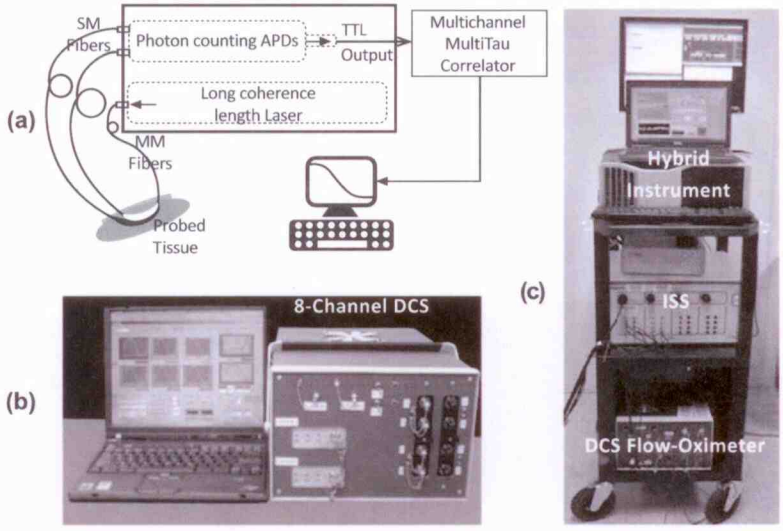

Fig. (3). (**a**) Schematic diagram of a typical DCS system. (**b**) A photograph of the portable 8-channel DCS system. (**c**) Photograph of a hybrid diffuse optical system consisting of a DCS flow-oximeter and a frequency-domain tissue oximeter (Imagent, ISS Inc.).

2.3. DCS Instrumentation

Fig. (**3a**) shows the diagram of a typical DCS system. For DCS, a long coherence length laser light source must be employed. Output from the laser can be delivered to the tissue through a multimode optical fiber. Single-mode (or few-mode) fibers should be used to collect photons from a single (or a few) speckle(s) emitted from the tissue surface. Fast photon-counting avalanche photodiodes (APDs) (e.g., SPCM-AQR-12, Perkin Elmer, CA) are used as detectors. A multi-tau correlator board (Correlator.com, NJ) takes the TTL output from the APDs and calculates temporal intensity auto-correlation functions of the detected signal. The optical and electronic components are controlled through a computer.

Several research groups have applied DCS technologies in biological tissues [4, 5, 54, 55, 60, 63-65, 79]. To fully utilize the blood flow information provided by DCS, hybrid systems combining DCS and NIRS (see Fig. (**3c**)) have been demonstrated to provide more comprehensive information for calculation of tissue blood flow, blood oxygenation and oxygenation metabolism [4, 57, 60, 63, 64]. Additionally, a very compact DCS system can be designed by exploiting recent developments in novel solid-state laser technologies [79, 84]. Fig. (**3b**) shows a portable 8-channel DCS instru-

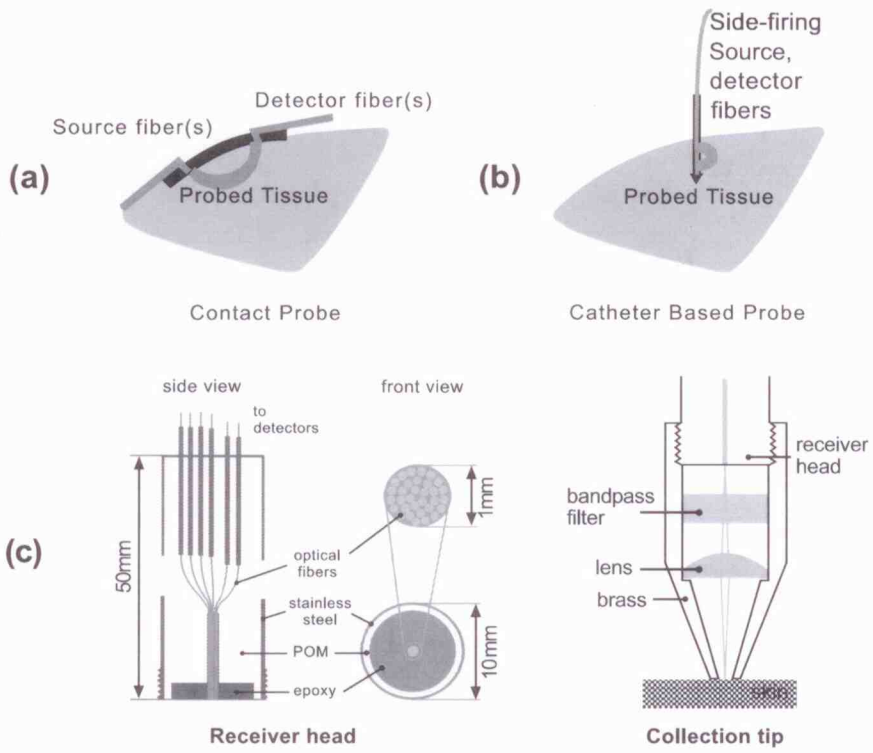

Fig. (4). Three schematic examples of DCS tissue probes: (**a**) contact probe, (**b**) side-illumination catheter-based probe, and (**c**) multi-fiber receiver head probe (reproduced from Fig. (**1**) in Reference [53]).

ment (Dimension: 18 cm × 28 cm × 33 cm). Recently Shang *et al* [79] demonstrated a dual wavelength 4-channel DCS flow-oximeter, which simultaneously measures tissue blood flow and blood oxygenation by a single compact device (see bottom of Fig. (**3c**)). Being truly portable, the DCS flow-oximeter is suitable for bed-side and *en route* monitoring of multiple hemodynamic parameters in tissue.

Similar to NIRS, DCS tolerates the usage of a wide variety of probes. The most basic probe employs one or more multimode source fibers and one or more single- or few-mode detector fibers. The fiber diameter of single- or few-mode detector fibers in DCS is limited to several micrometers. It has been previously shown that enlarging the fiber diameter (few-mode fibers) to cover multiple speckles increases the signal intensity, but also increases the noise proportionally and therefore does not necessarily result in much signal-to-noise-ratio improvement [71].

DCS can be used in many diverse situations requiring different probe designs to be utilized. Fig. (**4**) shows three example probes. The first probe (see Fig. (**4a**)) is a typical probe used in studies of human brain, tumors close to the body surface (e.g., breast tumor, head/neck tumor), and skeletal muscles [4, 55]. Straight or 90° bent fibers are utilized. This probe can be made MRI compatible [61, 96]. The second type of probe (see Fig. (**4b**)) consists of multiple side-firing fibers embedded in a catheter which could be inserted into tissues [3] or sutured onto the tissue surface. Finally, the third probe (see Fig. (**4c**)) is a multi-fiber receiver head probe utilized by Gisler and co-workers that employs up to thirty-two few-mode fibers to detect light from multiple speckles simultaneously [53]. Their goal was to maximize the number of detected photons per fiber by utilizing few-mode fibers and acquiring many correlation functions in parallel. With this approach, they have reduced the integration time down to 6.5 ms and are able to resolve changes in blood flow due to arterial pulsation in an analogous fashion to pulse-oximetry.

Practically all innovations from the design of NIRS probes can be taken and adapted for DCS use, and hybrid probes for both NIRS and DCS can be easily built by adding extra source and/or detector fibers.

3. CLINICAL APPLICATION EXAMPLES OF DCS

3.1. Cancer Diagnosis and Therapy Monitoring

Abnormal tissue hemodynamics and metabolism in tumor may precede detectable morphological changes of tumor, thus providing early diagnostic information. Also, measurement of tissue/tumor hemodynamic changes during cancer treatment is particularly attractive for cancer therapies that require tissue oxygen for treatment efficacy [5]. For example, patients with hypoxic tumors are well known to show only minimal improvements in response to radiation and photodynamic therapies [97-99]. Furthermore, cancer therapy can alter tumor hemodynamic/metabolic status, which further impacts treatment outcomes. Expectations are that functional assessment of tumor hemodynamic status before and during cancer therapy may provide information useful for early prediction of long-term treatment outcomes, thus enabling clinicians to optimize and individualize treatment.

DCS has been utilized in the monitoring of various tumor conditions including tumor contrast in breast cancer [65, 84],

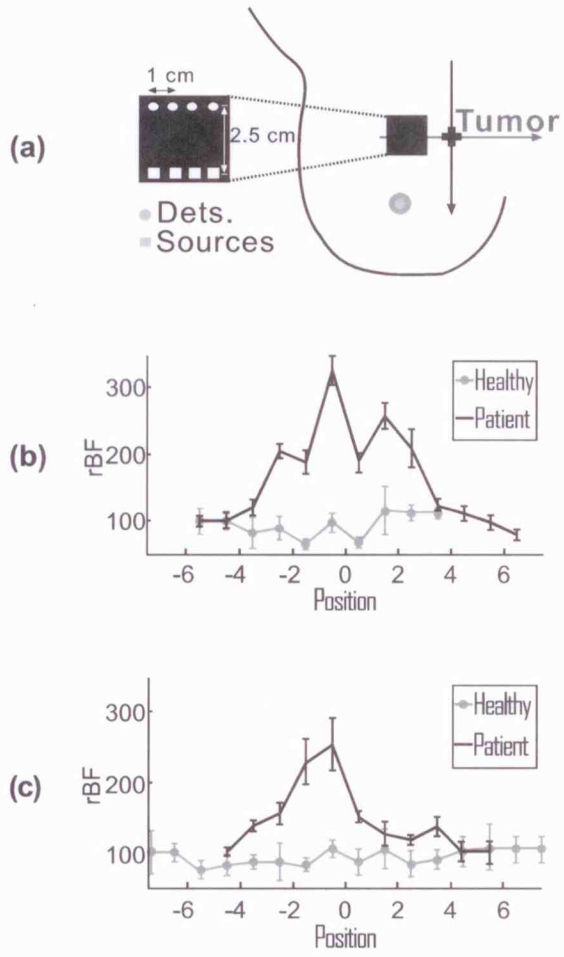

Fig. (5). (**a**) Hand-held probe with four source-detector pairs is scanned horizontally and vertically in 1 cm increments spanning the estimated tumor region as well as the surrounding healthy tissue. Relative blood flow (rBF) scans from one patient with a malignant tumor and a healthy volunteer are shown for both (**b**) horizontal and (**c**) vertical scans. Probe position is indicated relative to expected tumor center (position 0). Courtesy of T. Durduran [65].

early physiological changes in breast cancer in response to chemotherapy [84], the effects of chemo-radiation therapy on head/neck cancer [75], hemodynamic response to photodynamic therapy (PDT) in prostate cancer [3, 100], and the efficacy of PDT in murine tumor models [5, 56, 101-104]. This subsection begins with an example that demonstrates the clinical use of DCS for diagnosis of human breast tumors. A series of clinical translational studies using DCS for monitoring and evaluation of various cancer therapies in humans are then described.

Blood Flow Contrast in Breast Cancer. DCS has been tested for use in diagnosis of cancers [65, 84]. One such example is in the detection of tumor-to-normal flow contrast in breast tumors. In this case two healthy subjects and 5 patients with palpable breast tumors were recruited [65]. To increase tumor accessibility subjects were asked to lie supine, thus flattening the breast. An experienced researcher scanned the tumor with a hand-held optical probe (see Fig. (**4a**) and Fig. (**5a**)) in both horizontal and vertical directions in 1 cm increments across the tumor. Since probe pressure may induce signal variations two scan directions were used. This also allowed for checking the repeatability of the signal. For healthy volunteers, an arbitrary region was drawn as the tumor site, and a measurement was obtained by scanning across that region. This control measurement provided some information about the heterogeneity of blood flow in healthy breast tissue.

Only four of the source-detector positions, directly across from each other (separation of 2.5 cm), were used at each scanned position. The resultant correlation functions were then fit to a solution of the correlation diffusion equation to obtain a blood flow index. The results were normalized to the mean value of the measurements of the healthy tissue and the standard deviation was reported as the error bar. The averaged relative blood flow (%rBF) was reported at each position.

Fig. (**5**) shows horizontal (**b**) and vertical (**c**) profiles from one malignant tumor and one healthy breast. There was only slight variation observable in the healthy breast, whereas blood flow increased in both scan directions as the probe crossed over the tumor. Consequently, the contrast observed was attributable to the tumor and not the natural heterogeneity of the breast.

Patients were categorized into three groups: (1) a group with very little heterogeneity, i.e., the healthy breasts (2.7% variation, n = 2); (2) a group wherein the blood flow increased up to 230% of that of healthy tissue, i.e., malignant tumors (n = 2); and (3) a group wherein a moderate increase up to 153% was observed, i.e., benign tumors (n = 3). Although the power of the statistics of this study was not enough to conclude that differentiation can be achieved, these results are in qualitative agreement with previous Doppler ultrasound and PET [105-110] results where ~470-550% increases in blood flow were reported in malignant tumors with smaller contrasts in benign cases [108]. It is clearly demonstrated from these findings that robust flow contrasts in palpable tumors can be detected by DCS.

Breast Cancer Hemodynamic and Metabolic Contrasts in Response to Chemotherapy. This was a case study of a breast cancer patient during the early stages of neoadjuvant chemotherapy [84]. Both DCS and NIRS measurements were obtained simultaneously (using a hybrid instrument) on the same patient to derive information about tumor blood flow, blood oxygenation and oxygen metabolism. Tumor/normal contrast was scanned using a hand-held probe consisting of source and detector fibers, which is similar to the probe shown in Fig. (**5a**). The source-detector separations were 2.8 cm for NIRS and 2.5 cm for DCS. The scanning procedure was the same as shown in Fig. (**5a**).

As early as 3 days post-therapy significant changes in tumor hemodynamic parameters were detected. Fig. (**6**) presents line scans of the blood flow index (BFI = αD_b, Fig. (**6a**)) and total hemoglobin concentration (ctTHb, Fig. (**6b**)) from both the tumor breast and the contralateral breast before and after the first week of chemotherapy treatment (days 0, 3, and 7). Within the first week of treatment (day 7) NIRS revealed significant changes in tumor/normal contrast of total hemoglobin concentration ($rctTHb_{T/N}$ = 72 ± 17%) compared to pre-treatment value. Similarly, DCS found sig-

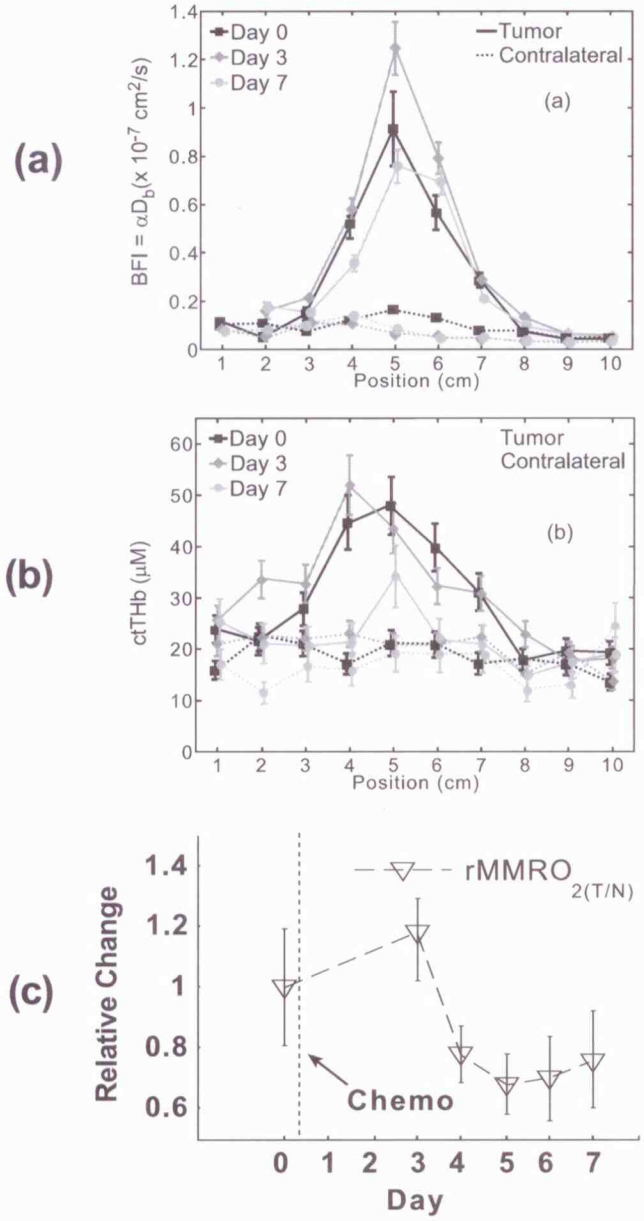

Fig. (6). Line scans of (**a**) BFI and (**b**) ctTHb before and after the first chemotherapy cycle (day 0, day 3, and day 7). On the tumor side of the breast, BFI showed clear contrast, which was much larger than the heterogeneity of the breast tissue on the contralateral side. The ctTHb also showed clear contrast on the tumor. Tumor contrasts changed in response to the chemotherapy. Error bars represent the standard deviation of repeated measurements. Plots were slightly offset along the *x* axis for better illustration of the error bars. (**c**) Relative metabolic rate of oxygen contrast ($rMMRO_{2(T/N)}$) in response to chemotherapy. The contrasts were calculated as the ratio of the average tumor value (positions 3 to 7 in Fig. (**6a**) and Fig. (**6b**)) in the line scans to the average value of the normal tissue on the same side of the breast (positions 8 to 10 in Fig. (**6a**) and Fig. (**6b**)). The contrasts were then normalized to the pre-chemotherapy values to reflect relative changes. Courtesy of C. Zhou [84].

nificant changes in tumor/normal flow contrast ($rBF_{T/N}$ = 75 ± 7% on day 7).

Fig. (**6c**) displays the relative changes in tumor/normal contrast of the mammary metabolic rate of oxygen ($rMMRO_{2(T/N)}$). $rMMRO_{2(T/N)}$ showed an initial increase (118 ± 13%, p = 0.68), which was most probably a result of the initial blood flow increase, although in order to confirm this hypothesis further evidence is necessary. However, after day 4, metabolic indices dropped significantly ($rMMRO_{2(T/N)}$ = 78 ± 7%, p = 0.05 on day 4) and then stabilized at this level until the end of the monitoring period.

In addition to the optical measurements, ultrasound and MRI measurements were performed before and after the completion of treatment and detected a decrease in tumor volume, indicating a partial response to therapy. The early hemodynamic responses to chemotherapy hold a potential for prediction of post-treatment outcomes (e.g., tumor volume change). This study also suggests that the combination of DCS and NIRS enhances treatment monitoring compared to either technique alone. The hybrid approach enables the construction of indices reflecting tissue metabolism, which may provide new insights about therapy mechanisms and outcomes.

Hemodynamic Monitoring of Head and Neck Tumor Undergoing Radiotherapy. This pilot study explored the potential of noninvasive DCS and NIRS for monitoring early relative blood flow (rBF), tissue oxygen saturation (StO_2) and total hemoglobin concentration (THC) responses to radiotherapy in patients with head and neck tumors. The rBF, StO_2 and THC in superficial neck tumor nodes of patients were measured before and throughout the radiation therapy period [75].

The protocol for this experiment consisted of pre-radiation measurements as baseline data, followed by weekly measurements for each individual until the treatment was completed. Each patient received daily fractionated radiation over 6.4 weeks and the optical measurements were completed just before treatment began each week. To obtain DCS and NIRS measurements a hand-held probe was placed on the neck tumor (see Fig. (**7a**)) and the forearm muscle (for control purposes) respectively. The largest source-detector separation of the probe was 3 cm for both optical techniques. Tumor/normal hemodynamic contrast was obtained by normalizing the tumor data to the arm muscle data.

The left panel of Fig. (**7**) shows the changes of rBF (**b**), StO_2 (**d**) and THC (**f**) averaged over seven patients who have complete responses (based on the tumor volume changes after treatment) to radiation therapy. Different patterns were exhibited from different individuals for the weekly rBF, StO_2, and THC kinetics, including significant early blood flow changes during the first two weeks. Average rBF increased (52.7 ± 9.7%) in the first week and decreased (42.4 ± 7.0%) in the second week. Average StO_2 increased from the baseline value of 62.9 ± 3.4% to 70.4 ± 3.2% at the end of the second week, and average THC showed a continuous decrease from the pretreatment value of 80.7 ± 7.0 μM to 73.3 ± 8.3 μM at the end of the second week and to 63.0 ± 8.1 μM at the end of the fourth week of therapy.

The right panel of Fig. (**7**) demonstrates the changes of rBF (**c**), StO_2 (**e**) and THC (**g**) observed from a partial responder. This patient exhibited substantially different tumor

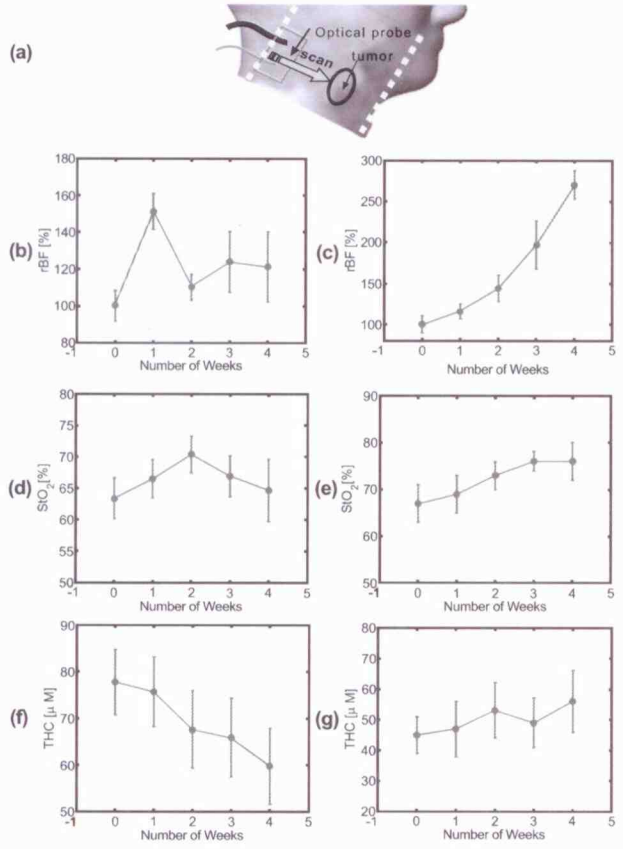

Fig. (7). (**a**) Hand-held probe for scanning the head/neck tumor. (**b**) Average tumor relative blood flow changes (rBF%) during radiotherapy averaged over seven patients who were complete responders to radiation treatment. Pretreatment value at week 0 was defined as 100% in all patients. (**d**) Average tumor blood oxygen saturation (StO_2). (**f**) Average tumor total hemoglobin concentration (THC). (**c**) rBF% observed from a partial responder. (**e**) StO_2 from a partial responder (**g**) THC from a partial responder. Courtesy of U. Sunar [75].

hemodynamic response during the therapy compared to the seven complete responders (see the left panel in Fig (**7**)); in this case *rBF* exhibited a continual increase, while StO_2 and *THC* also tended to increase over the course of treatment. For this patient, pre-therapy CT showed a large necrotic nodal mass, and the tumor was still relatively large and palpable at the end of the therapy. Postsurgical pathology confirmed the existence of residual tumor, and so the patient was considered to be a partial responder.

These preliminary data demonstrate the potential value of diffuse optical measurements for early prediction of cancer treatment outcomes (e.g., complete responders versus partial responders).

Real-time Monitoring of Human Prostate PDT. Preclinical PDT studies in murine tumors have found a strong correlation between tumor blood flow (rBF) changes during treatment and long-term treatment efficacy, indicative of the clinical dosimetry potential of DCS for prediction of cancer therapy efficacy [5]. The experiments discovered that the slope (flow reduction rate) over which rBF decreased during PDT was highly associated with treatment durability. These findings were consistent with the hypothesis that treatment efficacy is a function of tumor oxygenation during PDT; under oxygen-limited conditions (i.e., rapidly declining blood flow), treatment efficacy was abrogated.

Armed with promising results from the murine models above, Yu *et al.* [3] proceeded to adapt the DCS system for use in a Phase I clinical trial of interstitial human prostate PDT. A thin side-illumination fiber-optic probe (see Fig. (**4b**) and Fig. (**8a**)) containing source and detector fibers was constructed with multiple source-detector separations (0.5 to 1.5 cm) [3]. The fiber-optic probe was placed inside an 18-gauge catheter that had already been inserted into the patient's prostate gland. Five patients with locally recurrent prostate cancer in the Phase I trial of motexafin lutetium (MLu)-mediated PDT were measured using DCS and the side-illumination probe. The prostate was illuminated sequentially in several quadrants (e.g., Q1 to Q4) until the entire gland was treated.

Measured blood flow variation showed a similar trend in each individual. Fig. (**8b**) and Fig. (**8c**) show typical responses in blood flow over the course of PDT in two prostatic tumors. As was the case for murine tumors [5], a sharp decrease in prostate blood flow was observed [-41 ± 12 % (n = 5)], suggesting MLu-mediated PDT has an anti-vascular effect. The slope (flow reduction rate) during PDT showed large inter-prostate heterogeneities; 15%/min in Fig. (**8b**) versus 10%/min in Fig. (**8c**) measured from two prostates during PDT. On average (n = 5) the flow reduction rate from the five subjects was 12 ± 5 (%/minute).

Even though this study made no attempts to correlate clinical outcome with DCS-measured flow response during PDT, it is clear that PDT-induced flow responses hold potential for the prediction of treatment outcomes in humans, as shown in murine tumor models. The present study took a step in this direction.

3.2. Bedside Monitoring of Cerebral Physiology and Pathology

Noninvasive cerebral blood flow (CBF) measurements provide physiological insight critical for both pre-clinical models and in clinical applications. DCS was first utilized in rat brain models [63, 64, 111] in a monitoring capacity [64] and for demonstration of 3D DCS tomography [63, 71]. Utilization has also been extended into neonatal piglet models of head trauma, illustrating potential for continuous long term "bedside" monitoring [1]. In 2004, its use in human brain (through intact skull) was first demonstrated [57], and the techniques were later applied to functional studies of CBF in healthy adults [54, 55, 62]. In the clinical settings, DCS use has also been reported in premature infants [59, 60], neonates with congenital heart defects [96], adults with acute ischemic stroke [2] and traumatic brain injury patients [58]. This subsection consists of descriptions of several clinical examples where DCS was used for CBF measurement in patients with cerebral diseases.

Bedside Monitoring of Cerebrovascular Hemodynamics in Neuro-intensive Care Units. Optical scientists have identified an unfilled niche application for the DCS-NIRS hybrid approach as a bed-side monitor in adult neuro-intensive care

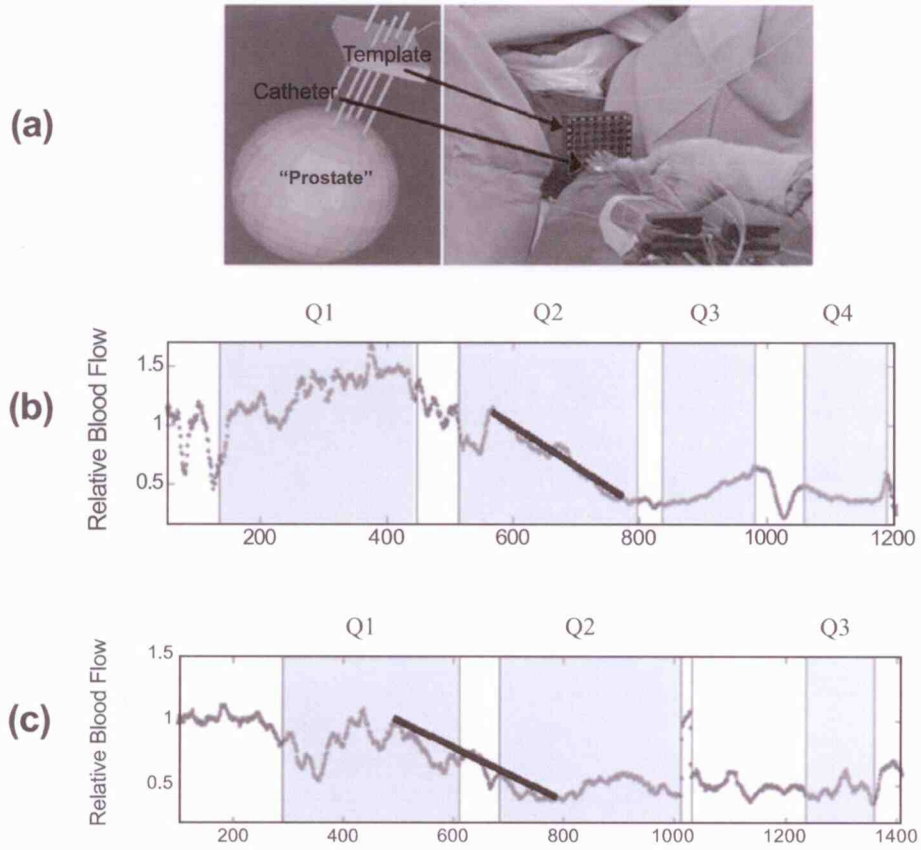

Fig. (8). (a) Custom-made template for guidance of placing catheters for prostate PDT. The treatment light was administered through the cylindrical diffusing fibers inside the catheters. The small side-illuminated probe was placed in the center of the prostate before PDT through one of the catheters. The catheter remained in place throughout PDT. (**b**) and (**c**) Tumor blood flow responses during PDT as a function of time measured from two prostates. Multiple quadrants of the prostates (e.g., Q1 to Q4) were illuminated sequentially until the entire gland was treated. The illumination periods are presented as shaded areas. Flow reduction rate is defined by the slope of the decrease in blood flow. This figure is reproduced from Fig. (**1**) and Fig. (**3**) in Reference [3].

units. For example, the hemodynamic responses of a cohort of acute ischemic stroke patients [2] and traumatic brain injury (TBI) patients [58] were studied using the optical methods. In TBI patients, DCS for blood flow measurement was validated against portable Xenon-CT [112] and concurred with invasive measurements of intracranial pressure, cerebral perfusion pressure and the partial pressure of oxygen during postural changes and hyperoxia.

For the acute ischemic stroke population, a mild orthostatic stress was induced by changing the head-of-bed position (HOB) as shown in Fig. (**9a**) [2]. With two probes being placed on the forehead near the frontal poles, CBF and hemoglobin concentrations were measured sequentially for 5 minutes at each of the following HOB positions: 30, 15, 0, -5 and 0 degrees, and then normalized to their values at 30 degrees. Fig. (**9b**, **left**) shows continuous CBF data taken over 25 minutes from a representative subject. The infarcted hemisphere (peri-infarct) shows a very large CBF increase in response to lowering of head-of-bed (HOB) position whereas the opposite hemisphere (contra-infarct) shows minimal changes that are similar to those observed on healthy people. While this was expected and observed in most (~75%) of the people (n = 17), others have shown a "paradoxical" response (see Fig. (**9b**, **right**)) where CBF decreased in response to lowering of the HOB position. Larger changes in peri-infarct hemisphere are presumably due to damaged cerebral autoregulation and are observed in both types of responses. The existence of the paradoxical response is an indicator for the potential usefulness of a bed-side monitor for individualized stroke care. In control populations [2, 113], both hemispheres behaved identically during the postural challenge, as expected. The example illustrates that diffuse optical instrumentation can be deployed at the neuro-intensive unit to directly monitor injured tissues.

Cerebral Metabolic Rate of Oxygen Consumption ($CMRO_2$) Estimates in Premature Infants. Roche-Labarbe et al [60] conducted experiments utilizing DCS in premature born infants (n = 11) and validated its use against transcranial Doppler ultrasound (TCD) measurements. In the report, the authors also demonstrated that the combination of NIRS and DCS to derive $CMRO_2$ could be more robust than NIRS-only models that they had utilized previously. They obtained measurements at multiple positions on the head and on a weekly basis for the first six weeks of life as shown in Fig. (**10**).

Interestingly, the total hemoglobin concentration and the blood oxygen-saturation (StO_2) decrease as the premature born infant matures over time. This is contrary to the increasing CBF as measured by DCS. Total hemoglobin concentration was converted to cerebral blood volume (CBV)

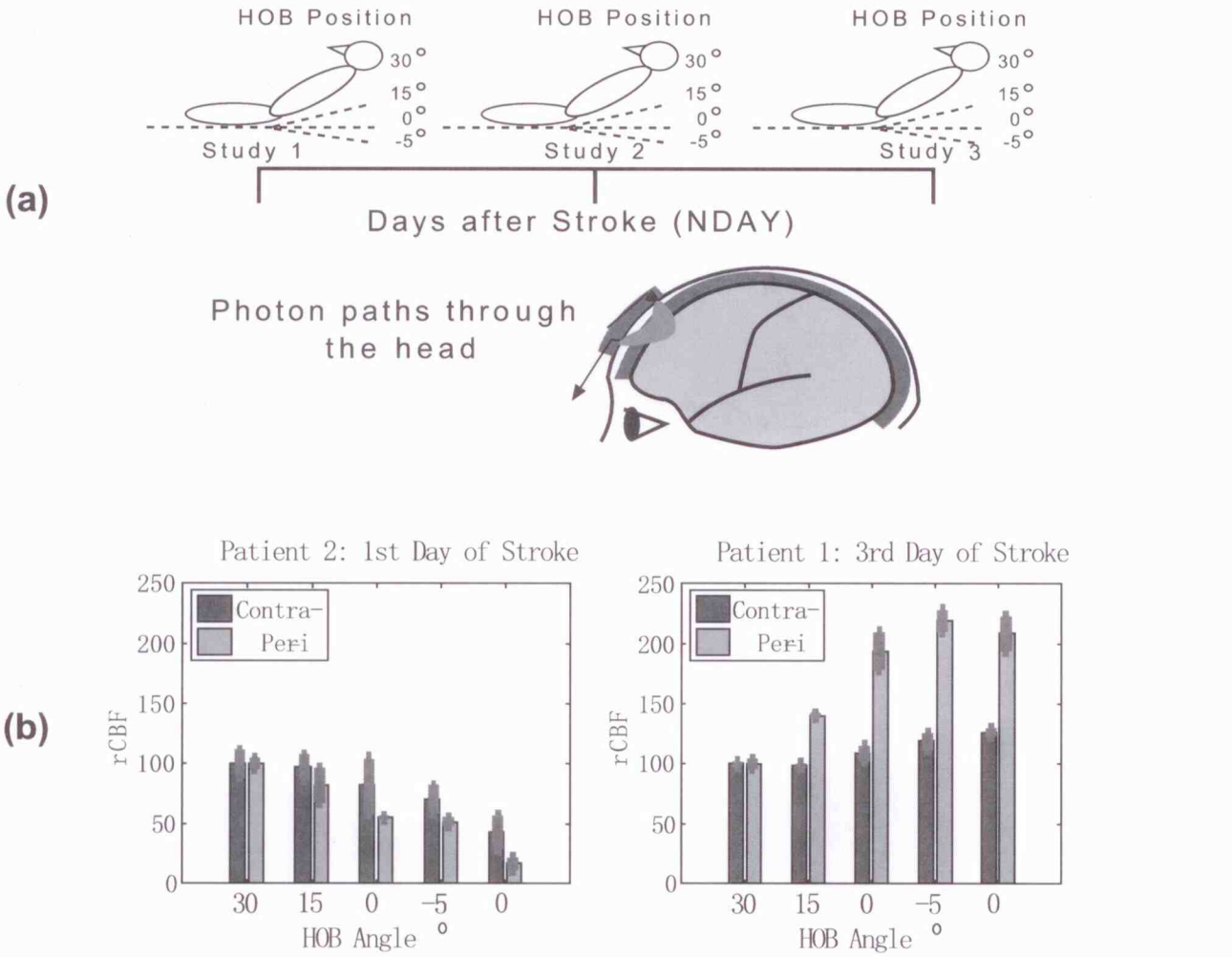

Fig. (9). (**a**) Measurement protocol and the probe positioning. (**b**) CBF data taken over 25 minutes from two representative subjects with stroke. A representative plot (**left**) was observed in about 75% of the subjects (n = 17); the infarcted hemisphere (peri-infarct) shows a very large CBF increase in response to lowering of HOB position. Others have shown a "paradoxical" response (**right**) where CBF decreased in response to lowering of the HOB position. This figure is reproduced from Fig. (**1**) in Reference [2].

utilizing a simple model, however, no trend was evident for CBV over time. Furthermore, making use of CBV to derive $CMRO_2$, as is done in NIRS-only approach, shows that both CBV and $CMRO_2$ appear unaltered over time. Conversely, if $CMRO_2$ is derived using NIRS-DCS hybrid data a linear increase with time is observed. This qualitatively agrees with physiological expectations dictating that CBF increases as StO_2 decreases; that is, oxygen utilization as well as oxygen metabolism should be increasing with the infant's age.

The authors argued that these findings demonstrate the robustness of the NIRS-DCS combined model (notice large error bars in sub-Fig. (**10f**)), which might be expected as this model relies on fewer approximations than the NIRS-only model [114]. Combining these results with other recent reports [96] of DCS-NIRS used in neonates to estimate $CMRO_2$, current research demonstrates the feasibility and importance of concurrent DCS and NIRS measurements.

3.3. Hemodynamic Evaluation of Ischemic Muscle and Revascularization Therapy

In situ quantification of the oxygen supply (blood flow) and metabolism in skeletal muscles with noninvasive optical methods has important clinical implications for understanding muscle physiology, screening of muscle vascular diseases such as the peripheral arterial disease (PAD), and evaluation of hemodynamic improvements in ischemic muscles after revascularization therapy. In a pilot study DCS was applied on human skeletal muscles, where the issues of light penetration and flow measurement sensitivity to deep muscle tissues were addressed experimentally by investigating tissue layer responses during prolonged cuff occlusion [4]. PAD and healthy legs were examined in terms of their different hemodynamic responses. Very recently, DCS was also used for continuous monitoring of acute hemodynamic improvements in ischemic muscles during arterial revascularization in patients with severe PAD. The results from these studies are described in this subsection.

Skeletal Muscle Layer Responses. A hybrid fiber-optic probe (see Fig. (**11a**) and Fig. (**4a**)) was taped on the top of calf muscle. The source-detector separations were 0.5, 1, 2, and 3 cm for DCS flow measurement, and 0.5, 1.5, and 4.0 cm for NIRS oxygenation measurement. According to diffusion theory, the light penetration depth depends on the tissue optical properties as well as source-detector separation. The

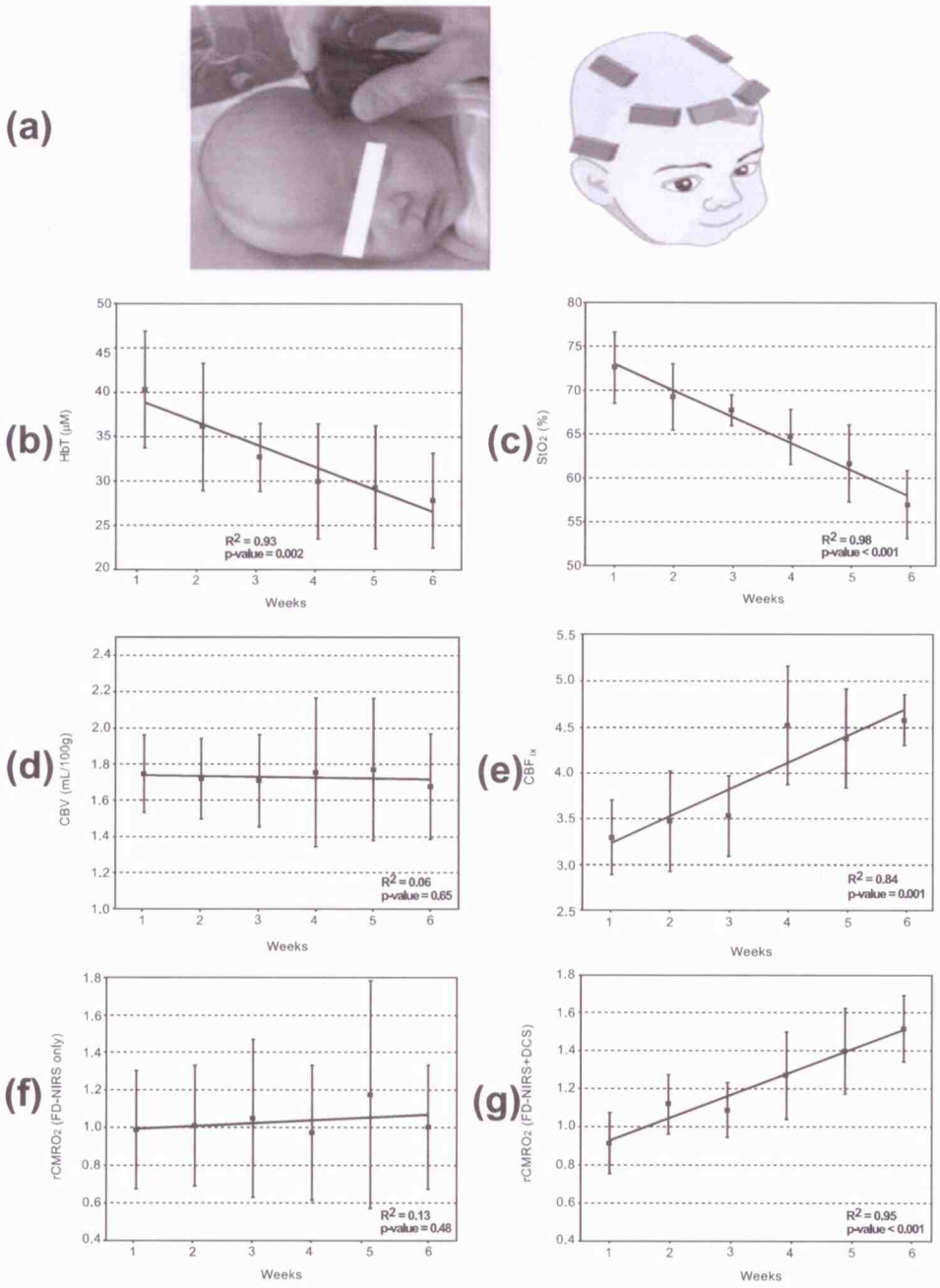

Fig. (10). (**a, left**) Photograph of a subject during optical measurement. (**a, right**) Locations of recording on the subject's head. (**b**) Average total hemoglobin concentration (HbT) as a function of age (n = 11); (**c**) Microvascular blood oxygen saturation (StO_2.) (**d**) Cerebral blood volume (CBV). (**e**) Cerebral blood flow index (CBFix). (**f**) $rCMRO_2$ estimated from FD-NIRS only. (**g**) $rCMRO_2$ calculated by combining FD-NIRS and DCS. Bold lines are linear regressions; R^2 and *P*-value of the regressions are in the bottom right corner of each graph. HbT and StO_2 decrease while CBF increases as the premature born infant matures over time. When HbT is converted to CBV, the trends vanish. Therefore if NIRS alone is used to derive $CMRO_2$, there are no trends in $CMRO_2$. However, if $CMRO_2$ is derived using NIRS-DCS hybrid data a linear increase with time is observed. This figure is reproduced from Fig. (**1**) and Fig. (**3**) in Reference [60].

penetration depth is typically in the order of one-third to one-half of the source-detector separation from the tissue surface.

Measurements were taken on ten healthy subjects and one patient with PAD. A 3-minute cuff occlusion protocol was used to investigate the responses in skeletal muscles at different layers in order to estimate light penetration depth and to validate results in the ischemic states. A Skinfold caliper was used to mechanically measure the thickness of the upper layers (skin and adipose tissues) on top of the muscle. The thickness of the upper layers above the leg flexors was 5.5 ± 0.4 mm (n = 10). Therefore, the optical signals detected from the large separations (≥ 2 cm) are mainly from the deep calf muscle.

Fig. (**11**) shows the typical responses of relative blood flow (rBF) and blood oxygen saturation (StO_2) during leg arterial occlusion from the different source-detector pairs on

a healthy individual. Source-detector pairs with large separations (≥ 2 cm) showed significantly stronger hemodynamic responses than those from the shortest source-detector separations (0.5 cm), consistent with the larger responses expected for muscle tissue as compared to the upper layers.

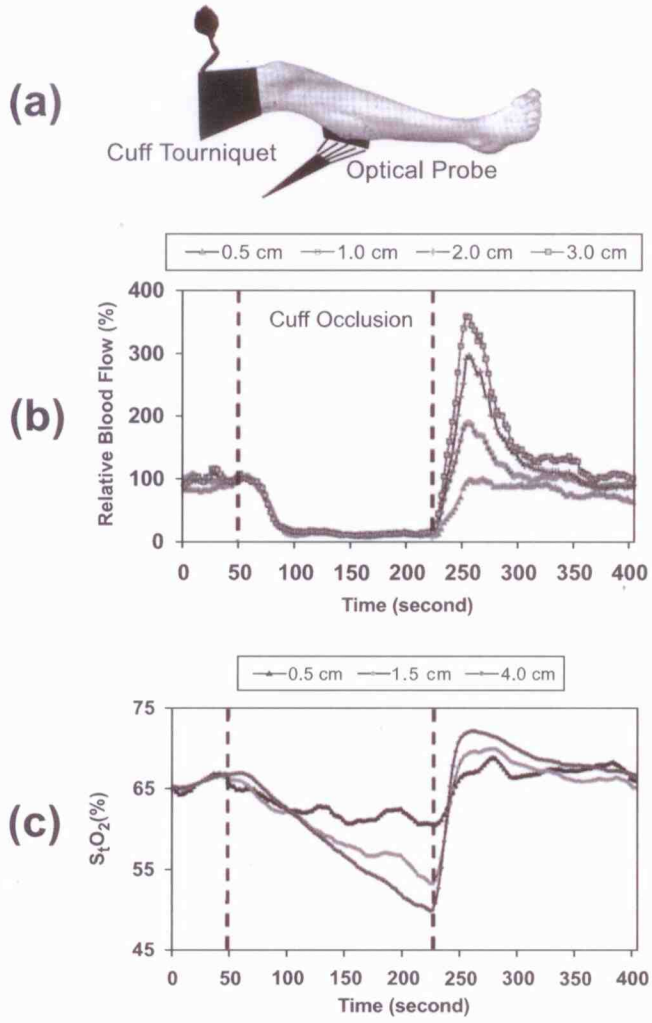

Fig. (11). (**a**) Cuff occlusion and the probe positioning. Representative curves of (**b**) relative blood flow (rBF) and (**c**) tissue blood oxygen saturation (StO_2) as function of time during arterial cuff occlusion. Data are shown from different source-detector pairs measured on a healthy leg. Vertical lines indicate the beginning and end of the occlusion period. Stronger reactive hyperemia after the release of occlusion, and de-oxygenation during occlusion were derived from source-detector pairs with larger separations. This figure is reproduced from Fig. (**3**) in Reference [4].

For healthy volunteers, similar responses were produced during cuff occlusion of the leg flexor muscles (see Fig. (**11**)). Trends in the PAD patient hemodynamic response (data not shown) were found to be similar to those of the healthy volunteers. Also, the arm muscles of healthy controls compared with that of the patient (data not shown) did not reveal any difference in their responses. However, in the PAD patient leg muscle, the relative magnitude of reactive hyperemia was ~1/2x of the controls and the recovery half-time of both StO_2 and rBF after occlusion were ~3x those of the controls.

Further investigations would test the capability of diffuse optical techniques for the screening and diagnosis of PAD. The community has also begun to consider DCS measurement during exercise, but these measurements can have motional artifacts; better understanding and characterization of these motional artifacts are needed.

Intraoperative Evaluation of Revascularization Effect on Ischemic Muscle. A portable DCS flow-oximeter (see Fig. (**3c**)) was recently used to continuously monitor flow and oxygenation changes in ischemic calf muscle throughout arterial revascularization at the bedside inside the operating rooms [81]. Prior to surgery, a fiber-optic probe (see Fig. (**11a**) and Fig. (**4a**)) was sterilized and taped on the surface of the calf muscle. The separation between the source and detector fibers was 2.5 cm. Calf muscle blood flow and oxygenation were continuously recorded before, during, and after the revascularization process. After revascularization, the relative change of blood flow (rBF), oxy-hemoglobin concentration $\Delta[HbO_2]$, and deoxy-hemoglobin concentration $\Delta[Hb]$ were averaged for 20 minutes and compared to the averaged 10-minute pre-revascularization baseline in order to evaluate the hemodynamic improvements in the calf muscle.

Fig. (**12**) shows a typical calf muscle hemodynamic response in a patient with PAD during femoroarterial bypass graft. When the femoral artery was clamped during the replacement of the occluded vessel, calf rBF decreased significantly, causing a gradual decrease/increase in $\Delta[HbO_2]/\Delta[Hb]$. The optical measurements demonstrate high sensitivity to dynamic physiological events (e.g., arterial clamping and releasing). The repair of the macro-circulation by revascularization resulted in the immediate blood flow improvement in muscle microvasculature. This result indicates an evident potential for objectively assessing the success of lower limb revascularization using diffuse optical techniques.

4. SUMMARY

The development and application of diffuse correlation spectroscopy (DCS) have been reviewed in this paper. DCS is an emerging technology which allows for the continuous detection of blood flow in deep tissues. In a relatively short time, the technique has been adopted by several research groups around the world from its theoretical conception to multiple clinical applications at the patient's bedside. DCS measurements show promise for the diagnosis of various diseases such as cancers, cerebral diseases, and PAD, and have potential for early prediction and longitudinal assessment of individual therapy outcomes.

DCS has many important advantages over one-time imaging modalities (e.g., MRI, PET, CT) in terms of being noninvasive, flexible, rapid, portable, inexpensive and continuous. It can be combined with other modalities such as near-infrared spectroscopy or tomography, MRI, PET, and CT. Preliminary results suggest that there are no adverse effects to patient populations as a result of these optical measurements. However, it should be noted that previous DCS experiments in humans used small patient populations for short time frames (up to several weeks). Longitudinal

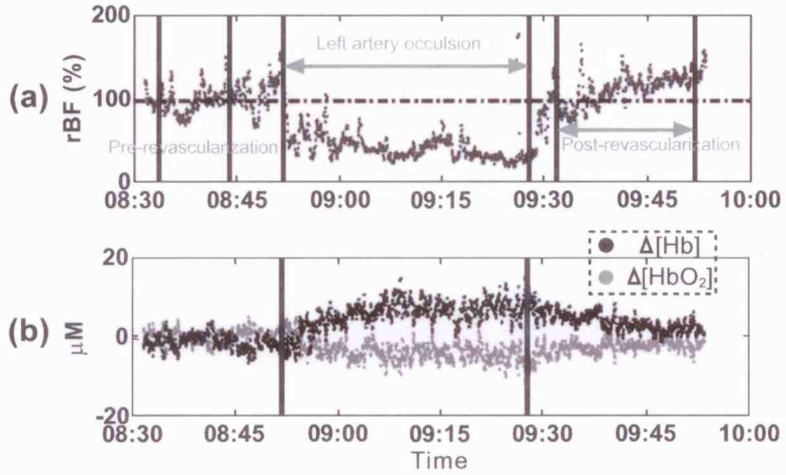

Fig. (12). Typical hemodynamic responses in calf muscle during femoral artery bypass graft: (**a**) rBF. (**b**) $\Delta[HbO_2]$ and $\Delta[Hb]$.

studies in large populations are needed to transfer this new technique into routine clinical use.

Some questions still remain unanswered about the DCS technique as applied to living tissue. For example, the interaction of photons with moving red blood cells in the complex environment of the tissue microvasculature is not completely understood. As such, a quantitative microscopic explanation about why Brownian-motion like autocorrelation curves work so effectively is still sought by researchers in the field. While empirical approaches to defining blood flow indices have been adopted and extensively cross-validated, it remains desirable to generate a more fundamental understanding of the origins of this blood flow index. Motion artifacts represent another issue of importance for certain classes of studies, e.g., blood flow measurements during muscle exercise. Better characterization and modeling of motion artifacts are needed. It is expected, however, that with further improved physical understanding and with more clinical applications, DCS technology will emerge rapidly as the technique of choice for clinical investigation of hemodynamic responses.

CONFLICT OF INTEREST

The author reports no conflicts of interest.

ACKNOWLEDGEMENTS

The author thanks the support by National Institution of Health (NIH) R21-HL083225, R21-AR062356 and R01-CA149274. American Heart Association (AHA) BGIA 2350015 and 0665446U, Department of Defense (DOD) W81XWH-04-1-0006, and the University of Kentucky Research Support Funds. The author also gratefully acknowledges discussions and interactions with numerous scientists in the biomedical optics community, including David Boas, Erin Buckley, Theresa Busch, Britton Chance, Cecil Cheung, Joseph Culver, Ran Cheng, Regine Choe, John Detre, Lixin Dong, Turgut Durduran, Douglas Fraker, Thomas Floyd, Joel Greenberg, Steven Hahn, Daniel Irwin, Andrew Kofke, Daniel Kameny, Meeri Kim, Daniel Licht, Gwen Lech, Emilie Mohler, Susan Margulies, Goro Nishimura, Harry Quon, Mark Rosen, Mitchell Schnall, Ulas Sunar, Yu Shang, Bruce Tromberg, Jionjiong Wang, Xiaoman Xing, Arjun Yodh, Chao Zhou, and Leonid Zubkov.

REFERENCES

[1] Zhou C, Eucker S, Durduran T, *et al.* Diffuse Optical Monitoring of Hemodynamic Changes in Piglet Brain with Closed Head Injury. Journal of Biomedical Optics. 2009; 14(034015).

[2] Durduran T, Zhou C, Edlow BL, *et al.* Transcranial optical monitoring of cerebrovascular hemodynamics in acute stroke patients. Opt Express. 2009 Mar 2; 17(5): 3884-902.

[3] Yu G, Durduran T, Zhou C, *et al.* Real-time in situ monitoring of human prostate photodynamic therapy with diffuse light. Photochem Photobiol. 2006 Sep-Oct; 82(5): 1279-84.

[4] Yu G, Durduran T, Lech G, *et al.* Time-dependent blood flow and oxygenation in human skeletal muscles measured with noninvasive near-infrared diffuse optical spectroscopies. J Biomed Opt. 2005 Mar-Apr; 10(2): 024027.

[5] Yu G, Durduran T, Zhou C, *et al.* Noninvasive monitoring of murine tumor blood flow during and after photodynamic therapy provides early assessment of therapeutic efficacy. Clin Cancer Res. 2005 May 1; 11(9): 3543-52.

[6] Wintermark M, Sesay M, Barbier E, *et al.* Comparative Overview of Brain Perfusion Imaging Techniques. Stroke. 2005; 36: 83-99.

[7] Baron JC. Mapping the ischaemic penumbra with PET: implications for acute stroke treatment. 1999; 9(4): 193-201.

[8] Mahagne MH, David O, Darcourt J, *et al.* Voxel-based mapping of cortical ischemic damage using Tc 99m L,L-ethyl cysteinate dimer SPECT in acute stroke. 2004; 14(1): 23-32.

[9] Latchaw RE, Yonas H, Hunter GJ, *et al.* Guidelines and recommendations for perfusion imaging in cerebral ischemia: A scientific statement for healthcare professionals by the writing group on perfusion imaging, from the Council on Cardiovascular Radiology of the American Heart Association. Stroke. 2003; 34(4): 1084-104.

[10] Wintermark M, Maeder P, Verdun FR, *et al.* Using 80 kVp versus 120 kVp in perfusion CT measurement of regional cerebral blood flow. American Journal of Neuroradiology. 2000 Nov-Dec; 21(10): 1881-4.

[11] Kidwell CS, Alger JR, Saver JL. Beyond mismatch: evolving paradigms in imaging the ischemic penumbra with multimodal magnetic resonance imaging. Stroke. 2003; 34: 2729-35.

[12] Detre JA, Leigh JS, Williams DS, Koretsky AP. Perfusion imaging. Magn Reson Med. 1992; 23(1): 37-45.

[13] Williams DS, Detre JA, Leigh JS, Koretsky AP. Magnetic resonance imaging of perfusion using spin inversion of arterial water. PNAS. 1992; 89: 212-6.

[14] Liu DL, Svanberg K, Wang I, Andersson-Engels S, Svanberg S. Laser Doppler perfusion imaging: new technique for determination of perfusion and reperfusion of splanchnic organs and tumor tissue. Lasers Surg Med. 1997; 20(4): 473-9.

[15] Durduran T, Burnett MG, Yu G, *et al.* Spatiotemporal quantification of cerebral blood flow during functional activation in rat somatosensory cortex using laser-speckle flowmetry. J Cereb Blood Flow Metab. 2004 May; 24(5): 518-25.

[16] Dunn AK, Bolay T, Moskowitz MA, Boas DA. Dynamic imaging of cerebral blood flow using laser speckle. Journal of Cerebral Blood Flow and Metabolism. 2001 MAR; 21(3): 195-201.

[17] Chen Z, Milner TE, Wang X, Srinivas S, Nelson JS. Optical Doppler tomography: imaging *in vivo* blood flow dynamics following pharmacological intervention and photodynamic therapy. Photochem Photobiol. 1998 Jan; 67(1): 56-60.

[18] Jobsis FF. Noninvasive infrared monitoring of cerebral and myocardial sufficiency and circulatory parameters. Science. 1977; 198: 1264-7.

[19] Jobsis-vanderVliet FF. Discovery of the near-infrared window into the body and the early development of near-infrared spectroscopy. Journal of Biomedical Optics. 1999 Oct; 4(4): 392-6.

[20] Yodh A, Chance B. Spectroscopy and Imaging with Diffusing Light. Physics Today. 1995 MAR; 48(3): 34-40.

[21] Chance B, Alfano R, editors. Proceedings of Optical Tomography, Photon Migration, and Spectroscopy of Tissue and Model Media: Theory, Human Studies, and Instrumentation1995: SPIE.

[22] Patterson MS, Moulton JD, Wilson BC, Berndt KW, Lakowicz JR. Frequency-Domain Reflectance for the Determination of the Scattering and Absorption Properties of Tissue. Applied Optics. 1991 NOV 1; 30(31): 4474-6.

[23] Patterson MS, Chance B, Wilson BC. Time resolved reflectance and transmittance for the non-invasive measurement of tissue optical properties. Applied Optics. 1989; 28: 2331-6.

[24] Gratton E, Mantulin W, Ven MJ, *et al.* The possibility of a near-infrared imaging system using frequency-domain methods. Hamamatsu, Japan. 1990: 183-9.

[25] Delpy DT, Cope M, van der Zee P, al e. Estimation of optical pathlength through tissue from direct time of flight measurement. Phys Med Biol. 1988; 33: 1433-42.

[26] Jacques SL. Time-resolved reflectance spectroscopy in turbid tissues. IEEE Transactions on Biomedical Engineering. 1989; 36: 1155-61.

[27] Benaron DA, Stevenson DK. Optical Time-of-Flight and Absorbency Imaging of Biologic Media. Science. 1993 MAR 5; 259(5100): 1463-6.

[28] O'Leary MA, Boas DA, Chance B, Yodh AG. Refraction of Diffuse Photon Density Waves. Physical Review Letters. 1992 NOV 2; 69(18): 2658-61.

[29] O'Leary MA, Boas DA, Chance B, Yodh AG. Refraction of Diffuse Photon Density Waves. Biophysical Journal. 1993 FEB; 64(2): A357-A.

[30] Boas DA, O'leary MA, Chance B, Yodh AG. Scattering and Wavelength Transduction of Diffuse Photon Density Waves. Physical Review E. 1993 MAY; 47(5): R2999-R3002.

[31] Fishkin JB, Gratton E. Propagation of photon density waves in strongly scattering media containing an absorbing 'semi-infinite' plane bounded by a straight edge. J Opt Soc Am A. 1993; 10: 127-40.

[32] Schmitt JM, Knuttel A, Knutson JR. Interference of diffusive light waves. J Opt Soc Am A. 1992; 9: 1832.

[33] Tromberg BJ, Svaasand LO, Tsay T, Haskell RC. Properties of photon density waves in multiple-scattering media. Applied Optics. 1993; 32: 607-16.

[34] Sevick EM, Lakowicz JR, Szmacinski H, Nowaczyk, Johnson ML. Frequency domain imaging of absorbers obscured by scattering. J Photochem Photobiol B: Biol. 1992; 16: 169-85.

[35] Johnson CC. Optical diffusion in blood. IEEE Transactions on Biomedical Engineering. 1970; BME17: 129-33.

[36] Ishimaru A. Wave Propagation and Scattering in Random Media. San Diego: Academic Press, Inc.; 1978.

[37] Furutsu K. On the diffusion equation derived from the space-time transport equation. J Opt Soc Am A. 1980; 70: 360.

[38] Groenhuis RAJ, Ferwerda, H.A., Ten Bosch, J.J. Scattering and absorption of turbid materials determined from reflection measurements. I. Theory. Applied Optics. 1983; 22: 2456-62.

[39] Yodh AG, Boas DA. Functional Imaging with Diffusing Light. In: Vo-Dinh T, editor. Biomedical Photonics Handbook: CRC Press; 2003. p. 21/1-45.

[40] Fantini S, Hueber D, Franceschini MA, *et al.* Non-invasive optical monitoring of the newborn piglet brain using continuous-wave and frequency-domain spectroscopy. Phys Med Biol. 1999; 44(6): 1543-63.

[41] Wolf M, Franceschini MA, Paunescu LA, *et al.* Absolute frequency-domain pulse oximetry of the brain: methodology and measurements. Adv Exp Med Biol. 2003; 530: 61-73.

[42] Habazettl H, Athanasopoulos D, Kuebler WM, *et al.* Near-infrared spectroscopy and indocyanine green derived blood flow index for noninvasive measurement of muscle perfusion during exercise. J Appl Physiol. 2010 Apr; 108(4): 962-7.

[43] Keller E, Nadler A, Alkadhi H, Kollias SS, Yonekawa Y, Niederer P. Noninvasive measurement of regional cerebral blood flow and regional cerebral blood volume by near-infrared spectroscopy and indocyanine green dye dilution. Neuroimage. 2003 Oct; 20(2): 828-39.

[44] Boas DA, Yodh AG. Spatially varying dynamical properties of turbid media probed with diffusing temporal light correlation. Journal of the Optical Society of America A-Optics Image Science and Vision. 1997 JAN; 14(1): 192-215.

[45] Tong P, Goldburg WI, Chan CK, Sirivat A. Turbulent transition by photon-correlation spectroscopy. Phys Rev A. 1988; 37: 2125-33.

[46] Tanaka T, Riva C, Ben-Sira I. Blood velocity measurements in human retinal vessels. Science. 1974; 186: 830-1.

[47] Stern MD. *In vivo* evaluation of microcirculation by coherent light scattering. Nature. 1975; 254: 56-8.

[48] Pine DJ, Weitz DA, Chaikin PM, Herbolzheimer. Diffusing-wave spectroscopy. Phys Rev Lett. 1988; 60: 1134-7.

[49] Maret G, Wolf PE. Multiple light scattering from disordered media. The effect of brownian motion of scatterers. Z Phys B. 1987; 65: 409-13.

[50] Boas DA, Campbell LE, Yodh AG. Scattering and Imaging with Diffusing Temporal Field Correlations. Physical Review Letters. 1995 AUG 28; 75(9): 1855-8.

[51] Feke GT, Riva CE. Laser Doppler Measurements of Blood Velocity in Human Retinal-Vessels. Journal of the Optical Society of America. 1978; 68(4): 526-31.

[52] Stephen MJ. Temporal fluctuations in wave propagation in random media. PhysRevB. 1988; 37: 1-5.

[53] Dietsche G, Ninck M, Ortolf C, Li J, Jaillon F, Gisler T. Fiber-based multispeckle detection for time-resolved diffusing-wave spectroscopy: characterization and application to blood flow detection in deep tissue. Appl Opt. 2007 Dec 10; 46(35): 8506-14.

[54] Li J, Dietsche G, Iftime D, *et al.* Noninvasive detection of functional brain activity with near-infrared diffusing-wave spectroscopy. Journal of Biomedical Optics. 2005 Jul-Aug; 10(4): 044002.

[55] Durduran T, Yu G, Burnett MG, *et al.* Diffuse optical measurement of blood flow, blood oxygenation, and metabolism in a human brain during sensorimotor cortex activation. Opt Lett. 2004 Aug 1; 29(15): 1766-8.

[56] Menon C, Polin GM, Prabakaran I, *et al.* An integrated approach to measuring tumor oxygen status using human melanoma xenografts as a model. Cancer Research. 2003 Nov; 63(21): 7232-40.

[57] Durduran T. Non-Invasive Measurements of Tissue Hemodynamics with Hybrid Diffuse Optical Methods [Ph.D. thesis]: University of Pennsylvania; 2004.

[58] Kim MN, Durduran T, Frangos S, *et al.* Noninvasive measurement of cerebral blood flow and blood oxygenation using near-infrared and diffuse correlation spectroscopies in critically brain-injured adults. Neurocrit Care. 2010 Apr; 12(2): 173-80.

[59] Buckley EM, Cook NM, Durduran T, *et al.* Cerebral hemodynamics in preterm infants during positional intervention measured with diffuse correlation spectroscopy and transcranial Doppler ultrasound. Optics Express. 2009 Jul; 17(15): 12571-81.

[60] Roche-Labarbe N, Carp SA, Surova A, *et al.* Noninvasive Optical Measures of CBV, StO2, CBF Index, and rCMRO2 in Human Premature Neonates' Brains in the First Six Weeks of Life. Human Brain Mapping. 2010; 31(3): 341-52.

[61] Yu G, Floyd T, Durduran T, *et al.* Validation of diffuse correlation spectroscopy for muscle blood flow with concurrent arterial spin labeled perfusion MRI. Optics Express. 2007; 15(3): 1064-75

[62] Li J, Ninck M, Koban L, Elbert T, Kissler J, Gisler T. Transient functional blood flow change in the human brain measured noninvasively by diffusing-wave spectroscopy. Opt Lett. 2008 Oct 1; 33(19): 2233-5.

[63] Culver JP, Durduran T, Furuya T, Cheung C, Greenberg JH, Yodh AG. Diffuse optical tomography of cerebral blood flow, oxygenation, and metabolism in rat during focal ischemia. Journal of Cerebral Blood Flow and Metabolism. 2003 AUG; 23(8): 911-24.

[64] Cheung C, Culver JP, Takahashi K, Greenberg JH, Yodh AG. *In vivo* cerebrovascular measurement combining diffuse near-infrared absorption and correlation spectroscopies. Physics in Medicine and Biology. 2001 AUG; 46(8): 2053-65.

[65] Durduran T, Choe R, Yu G, *et al.* Diffuse optical measurement of blood flow in breast tumors. Opt Lett. 2005 Nov 1; 30(21): 2915-7.

[66] Culver JP, Furuya D, Durduran T, Cheung C, Greenberg JH, Yodh AG. Diffuse optical measurement of hemoglobin and cerebral blood flow in rat brain during hypercapnia, hypoxia and cardiac arrest. In: Wilson DF, Evans SM, Biaglow J, Pastuszko A, editors. Adv Exp Biol, in Oxygen Transport to Tissue: Plenum Press; 2002. p. 293-8.

[67] Varma HM, Nandakumaran AK, Vasu RM. Study of turbid media with light: Recovery of mechanical and optical properties from boundary measurement of intensity autocorrelation of light. Journal of the Optical Society of America A-Optics Image Science and Vision. 2009 Jun; 26(6): 1472-83.

[68] Zhou C. *In-vivo* Optical Imaging and Spectroscopy of Cerebral Hemodynamics: PhD dissertation, University of Pennsylvania; 2007.

[69] Jaillon F, Skipetrov SE, Li J, Dietsche G, Maret G, Gisler T. Diffusing-wave spectroscopy from head-like tissue phantoms: influence of a non-scattering layer. Optics Express. 2006 Oct; 14(22): 10181-94.

[70] Gagnon L, Desjardins M, Jehanne-Lacasse J, Bherer L, Lesage F. Investigation of diffuse correlation spectroscopy in multi-layered media including the human head. Optics Express. 2008 Sep; 16(20): 15514-30.

[71] Zhou C, Yu G, Furuya D, Greenberg JH, Yodh AG, Durduran T. Diffuse optical correlation tomography of cerebral blood flow during cortical spreading depression in rat brain. Optics Express. 2006; 14: 1125-44.

[72] Boas DA, Culver JP, Stott JJ, Dunn AK. Three dimensional Monte Carlo code for photon migration through complex heterogeneous media including the adult human head. Optics Express. 2002 FEB 11; 10(3): 159-70.

[73] Cheung R, Solonenko M, Busch TM, *et al.* Correlation of *in vivo* photosensitizer fluorescence and photodynamic-therapy-induced depth of necrosis in a murine tumor model. Journal of Biomedical Optics. 2003 APR; 8(2): 248-52.

[74] Wang HW, Putt ME, Emanuele MJ, *et al.* Treatment-induced changes in tumor oxygenation predict photodynamic therapy outcome. Cancer Res. 2004 Oct 15; 64(20): 7553-61.

[75] Sunar U, Quon H, Durduran T, *et al.* Noninvasive diffuse optical measurement of blood flow and blood oxygenation for monitoring radiation therapy in patients with head and neck tumors: a pilot study. Journal of Biomedical Optics. 2006 Nov-Dec; 11(6).

[76] Sunar U, Rohrbach D, Rigual N, *et al.* Monitoring photobleaching and hemodynamic responses to HPPH-mediated photodynamic therapy of head and neck cancer: a case report. Opt Express. 2010 Jul 5; 18(14): 14969-78.

[77] Becker TL, Paquette AD, Keymel KR, Henderson BW, Sunar U. Monitoring blood flow responses during topical ALA-PDT. Biomed Opt Express. 2010; 2(1): 123-30.

[78] Shang Y, Cheng R, Dong L, Ryan SJ, Saha SP, Yu G. Cerebral monitoring during carotid endarterectomy using near-infrared diffuse optical spectroscopies and electroencephalogram. Phys Med Biol. 2011 May 21; 56(10): 3015-32.

[79] Shang Y, Zhao Y, Cheng R, Dong L, Irwin D, Yu G. Portable optical tissue flow oximeter based on diffuse correlation spectroscopy. Optics Letters. 2009 November 15, 2009; 34(20): 3556-8.

[80] Shang Y, Symons TB, Durduran T, Yodh AG, Yu G. Effects of muscle fiber motion on diffuse correlation spectroscopy blood flow measurements during exercise. Biomed Opt Express. 2010; 1(2): 500-11.

[81] Yu G, Shang Y, Zhao Y, Cheng R, Dong L, Saha SP. Intraoperative evaluation of revascularization effect on ischemic muscle hemodynamics using near-infrared diffuse optical spectroscopies. J Biomed Opt. 2011 Feb; 16(2): 027004.

[82] Belau M, Ninck M, Hering G, *et al.* Noninvasive observation of skeletal muscle contraction using near-infrared time-resolved reflectance and diffusing-wave spectroscopy. J Biomed Opt. 2010 Sep-Oct; 15(5): 057007.

[83] Xing X, Mohler ER, Zhou C, *et al.*, editors. Hemodynamic Changes in Diabetic Pig Muscle. SVMB 18th Annual Meeting 2007; Baltimore, MA.

[84] Zhou C, Choe R, Shah N, *et al.* Diffuse optical monitoring of blood flow and oxygenation in human breast cancer during early stages of neoadjuvant chemotherapy. J Biomed Opt. 2007 Sep-Oct; 12(5): 051903.

[85] Berne BJ, Pecora R. Dynamic Light Scattering with Applications to Chemistry, Biology, and Physics. Malabar, FL: Krieger; 1990.

[86] Chu B, editor. Laser light scattering: basic principles and practice. New York: Academic; 1991.

[87] Brown W. Dynamic Light Scattering: The Method and Some Applications. New York: Clarendon; 1993.

[88] Briers JD. Laser Doppler, speckle and related techniques for blood perfusion mapping and imaging. Physiol Meas. 2001 Nov; 22(4): R35-66.

[89] Boas DA, Meglinsky IV, Zemany L, Campbell LE, Chance B, Yodh AG. Diffusion of temporal field correlation with selected applications. Biophysical Journal. 1996 FEB; 70(2): Wp306.

[90] Eucker S, Ichord R, Friess S, *et al.* Direction dependence of rotational accelerational injury on cerebrovascular hemodynamics response depends on direction of angular acceleration. Journal of Neurotrauma. 2005 OCT; 22(10): 1254-.

[91] Boas D. Diffuse Photon Probes of Structural and Dynamical Properties of Turbid Media: Theory and Biomedical Applications [Ph.D.] Philadelphia: University of Pennsylvania, Dissertation; 1996.

[92] Ackerson BJ, Dougherty RL, Reguigui NM, Nobbman U. Correlation transfer: Application of radiative transfer solution methods to photon correlation problems. JThermophysand Heat Trans. 1992; 6: 577-88.

[93] Dougherty RL, Ackerson BJ, Reguigui NM, Dorri-Nowkoorani F, Nobbmann U. Correlation transfer: Development and application. JQuantSpectroscRadiatTransfer. 1994; 52: 713-27.

[94] Heckmeier M, Skipetrov SE, Maret G, Maynard R. Imaging of dynamic heterogeneities in multiple-scattering media. Journal of the Optical Society of America. 1997; 14(1): 185-91.

[95] Einstein A. On the Motion of Small Particles Suspended in Liquids at Rest Required by the Molecular-Kinetic Theory of Heat. Annalen der Physik. 1905; 17: 549-60.

[96] Durduran T, Zhou C, Buckley EM, *et al.* Optical measurement of cerebral hemodynamics and oxygen metabolism in neonates with congenital heart defects. J Biomed Opt. 2010 May-Jun; 15(3): 037004.

[97] Busch TM, Hahn SM, Evans SM, Koch CJ. Depletion of tumor oxygenation during photodynamic therapy: Detection by the hypoxia marker EF3 [2-(2-nitroimidazol-1[H]-yl)-N-(3,3,3-trifluoropropyl)acetamide]. Cancer Research. 2000 May; 60(10): 2636-42.

[98] Leach RM, Hill HS, Snetkov VA, Ward JPT. Hypoxia, energy state and pulmonary vasomotor tone. Respiratory Physiology & Neurobiology. 2002 Aug; 132(1): 55-67.

[99] Carlson DJ. Mechanism of intrinsic radiation sensitivity: the effects of DNA damage repair, oxygen, and radiation quality. West Lafayette: Purdue University; 2006.

[100] Du KL, Mick R, Busch T, *et al.* Preliminary results of interstitial motexafin lutetium-mediated PDT for prostate cancer. Lasers in Surgery and Medicine. 2006 Jun; 38(5): 427-34.

[101] Busch TM, Xing X, Yu G, *et al.* Fluence rate-dependent intratumor heterogeneity in physiologic and cytotoxic responses to Photofrin photodynamic therapy. Photochem Photobiol Sci. 2009; 8: 1683 - 93.

[102] Sunar U, Makonnen S, Zhou C, *et al.* Hemodynamic responses to antivascular therapy and ionizing radiation assessed by diffuse optical spectroscopies. Optics Express. 2007 Nov; 15(23): 15507-16.

[103] Song L, Li H, Sunar U, *et al.* Naphthalocyanine-reconstituted LDL nanoparticles for *in vivo* cancer imaging and treatment. Int J Nanomedicine. 2007; 2(4): 767-74.

[104] Cerniglia GJ, Pore N, Tsai JH, *et al.* Epidermal Growth Factor Receptor Inhibition Modulates the Microenvironment by Vascular Normalization to Improve Chemotherapy and Radiotherapy Efficacy. PLoS One. 2009; 4(8): e6539.

[105] Beaney RP, Lammertsma AA, Jones T, McKenzie CG, Halnan KE. Positron emission tomography for in-vivo measurement of regional blood flow, oxygen utilisation, and blood volume in patients with breast carcinoma. Lancet. 1984 Jan 21; 1(8369): 131-4.

[106] Wilson CB, Snook DE, Dhokia B, *et al.* Quantitative measurement of monoclonal antibody distribution and blood flow using positron emission tomography and 124iodine in patients with breast cancer. Int J Cancer. 1991 Feb 1; 47(3): 344-7.

[107] Wilson CB, Lammertsma AA, McKenzie CG, Sikora K, Jones T. Measurements of blood flow and exchanging water space in breast tumors using positron emission tomography: a rapid and noninvasive dynamic method. Cancer Res. 1992 Mar 15; 52(6): 1592-7.

[108] Madjar H, Sauerbrei W, Prompeler HJ, Wolfarth R, Gufler H. Color Doppler and duplex flow analysis for classification of breast lesions. Gynecol Oncol. 1997 Mar; 64(3): 392-403.

[109] Cosgrove DO, Bamber JC, Davey JB, McKinna JA, Sinnett HD. Color Doppler signals from breast tumors. Work in progress. Radiology. 1990 Jul; 176(1): 175-80.

[110] Kedar RP, Cosgrove DO, Smith IE, Mansi JL, Bamber JC. Breast carcinoma: measurement of tumor response to primary medical therapy with color Doppler flow imaging. Radiology. 1994 Mar; 190(3): 825-30.

[111] Culver JP, Siegel AM, Stott JJ, Boas DA. Volumetric diffuse optical tomography of brain activity. Optics Letters. 2003 NOV 1; 28(21): 2061-3.

[112] Kim MN, Durduran T, Frangos S, *et al.*, editors. Validation Of Diffuse Correlation Spectroscopy Against Xenon CTCBF In Humans After Traumatic Brain Injury or Subarachnoid 1 Hemorrhage. Neurocritical Care Society Annual Meeting; 2008; Miami, FL.

[113] Edlow BL, Kim MN, Durduran T, *et al.* The effect of healthy aging on cerebral and systemic hemodynamic responses to posture change. Brain 09; Chicago: International Society of Cerebral Blood Flow and Metabolism; 2009.

[114] Boas DA, Strangman G, Culver JP, *et al.* Can the cerebral metabolic rate of oxygen be estimated with near-infrared spectroscopy? Physics in Medicine and Biology. 2003 Aug; 48(15): 2405-18.

[115] Haskell RC, Svaasand LO, Tsay T, Feng T, McAdams MS, Tromberg BJ. Boundary conditions for the diffusion equation in radiative transfer. J Opt Soc Am A. 1994; 11: 2727-41.

Received: May 03, 2010 Revised: May 28, 2011 Accepted: June 11, 2011